

Effects of Supernova Feedback on the Formation of Galaxy Disks

Cecilia Scannapieco^{1*}, Patricia B. Tissera^{2,3}, Simon D.M. White¹ and Volker Springel¹

¹ *Max-Planck Institute for Astrophysics, Karl-Schwarzschild Str. 1, D85748, Garching, Germany.*

² *Instituto de Astronomía y Física del Espacio, Casilla de Correos 67, Suc. 28, 1428, Buenos Aires, Argentina.*

³ *Consejo Nacional de Investigaciones Científicas y Técnicas, CONICET, Argentina.*

2 February 2022

ABSTRACT

We use cosmological simulations in order to study the effects of supernova (SN) feedback on the formation of a Milky Way-type galaxy of virial mass $\sim 10^{12} h^{-1} M_{\odot}$. We analyse a set of simulations run with the code described by Scannapieco et al. (2005, 2006), where we have tested our star formation and feedback prescription using isolated galaxy models. Here we extend this work by simulating the formation of a galaxy in its proper cosmological framework, focusing on the ability of the model to form a disk-like structure in rotational support. We find that SN feedback plays a fundamental role in the evolution of the simulated galaxy, efficiently regulating the star formation activity, pressurizing the gas and generating mass-loaded galactic winds. These processes affect several galactic properties such as final stellar mass, morphology, angular momentum, chemical properties, and final gas and baryon fractions. In particular, we find that our model is able to reproduce extended disk components with high specific angular momentum and a significant fraction of young stars. The galaxies are also found to have significant spheroids composed almost entirely of stars formed at early times. We find that most combinations of the input parameters yield disk-like components, although with different sizes and thicknesses, indicating that the code can form disks without fine-tuning the implemented physics. We also show how our model scales to smaller systems. By analysing simulations of virial masses $10^9 h^{-1} M_{\odot}$ and $10^{10} h^{-1} M_{\odot}$, we find that the smaller the galaxy, the stronger the SN feedback effects.

Key words: galaxies: formation - evolution - abundances - cosmology: theory - methods: numerical

1 INTRODUCTION

The formation of spiral galaxies is currently a subject of considerable interest in cosmology. From a theoretical point of view, the formation of disk configurations is well understood as a result of specific angular momentum conservation during the collapse and relaxation of gas within dark matter potential wells (Fall & Efstathiou 1980; Mo, Mao & White 1998). Dark matter and baryons acquire similar specific angular momenta from tidal torques before collapse (Hoyle 1953; Peebles 1969; White 1984). Provided the gas conserves this angular momentum, its collapse leads to a disk-like configuration at the centre of its dark matter halo. If stars form from this rotationally supported gas, then spiral disks like those observed can develop. However, centrifugally supported stel-

lar disks are thickened or destroyed by rapid fluctuations in the gravitational potential such as those produced by the accretion of satellite galaxies (Toth & Ostriker 1992; Quinn, Hernquist & Fullagar 1993; Velazquez & White 1999). The presence of thin disks in many present-day spirals suggests that they had a relatively quiet mass accretion history, at least in the recent past.

Numerical simulations have become an important tool for studying galaxy formation due to their ability to describe the nonlinear, coupled evolution of dark matter and baryons in its cosmological context. However, this has turned out to be an extremely challenging problem because of the need to describe simultaneously the large-scale dynamics of galaxy assembly and the small-scale processes related to star formation and evolution. State-of-the-art simulations have implemented schematic recipes for radiative cooling, star formation, feedback from supernovae (SN), stellar winds, black

* E-mail: cecilia@mpa-garching.mpg.de

hole formation and active galactic nuclei. Although these are successful in many respects, they have had difficulty reproducing extended disk-dominated galaxies in typical dark matter haloes. The main problem is so-called *catastrophic angular momentum loss*, which arises when the baryonic components transfer most of their angular momentum to the dark matter during condensation into the central regions, forming dominant spheroidal stellar systems and disks that are too small compared to observations (e.g. Navarro & Benz 1991; Navarro & White 1994).

The formation of disks is heavily influenced by details of the gas cooling process. Disks that are less centrally concentrated and with higher specific angular momentum are obtained if cooling is artificially suppressed during the assembly of dark matter haloes (Weil, Eke & Efstathiou 1998; Eke, Efstathiou & Wright 2000). Many recent studies have attempted to prevent the early cooling of gas and the loss of angular momentum, some of them successfully reproducing disks as big as observed spirals (e.g. Abadi et al. 2003; Governato et al. 2004; Robertson et al. 2004; Okamoto et al. 2005; Governato et al. 2007). These studies have pointed out the importance of stellar feedback as a key process providing pressure support to the gas and preventing its rapid collapse within the haloes, thereby regulating star formation activity. However, it seems that fine-tuning of the models is required in order to reproduce the observed properties of disk galaxies in a hierarchical scenario, and a detailed understanding of disk formation remains elusive. Insufficient numerical resolution or a poor description of the interstellar medium (which influences the efficiency of the stellar feedback) have also been proposed as causes for the inability to reproduce convincing disk galaxies in simulations (e.g. Okamoto et al. 2003; Governato et al. 2004).

Over the years, many authors have included star formation and feedback recipes both in mesh-based and in SPH codes in order to study the effects of SN feedback on galaxy properties such as star formation histories, metallicity evolution, generation of galactic outflows, abundance of satellites and galaxy scaling relations (e.g. Katz & Gunn 1991; Cen & Ostriker 1992; Navarro & White 1993; Metzler & Evrard 1994; Steinmetz & Müller 1995; Gerritsen & Icke 1997; Yepes et al. 1997; Cen & Ostriker 1999; Sommer-Larsen, Gelato & Vedel 1999; Thacker & Couchman 2000; Kay et al. 2002; Semelin & Combes 2002; Abadi et al. 2003; Marri & White 2003; Sommer-Larsen, Götz & Portinari 2003; Springel & Hernquist 2003; Brook et al. 2004; Okamoto et al. 2005; Oppenheimer & Davé 2006; Stinson et al. 2006; Governato et al. 2007; Dalla Vecchia & Schaye 2008; Dubois & Teyssier 2008; Finlator & Davé 2008). All these feedback implementations require arbitrary and *ad hoc* elements because the relevant dynamical processes cannot be resolved by the simulations and so have to be introduced as “sub-grid” models. As a result, their validity is uncertain and the conclusions to be drawn from their successes and failures are correspondingly unclear. A further difficulty is introduced by numerical limitations which have so far prevented the simulation at high resolution of a large and representative sample of galaxies in their proper cosmological setting; typically, the evolution of a small number of selected objects is studied in detail, often chosen as those most likely to produce disk galaxies. It is thus uncertain whether existing models can successfully reproduce the variety of disk galaxies observed in the Uni-

verse. In particular, no Λ CDM simulation has yet managed to produce a late-type spiral like M33 or M101.

In Scannapieco et al. (2005, 2006), we have presented a new model for the effects of SN feedback in cosmological simulations. This model was implemented within the Tree-PM SPH code GADGET-2 (Springel & Hernquist 2002; Springel 2005), and is described in detail in Scannapieco et al. (2005, 2006). Our model includes a scheme to treat a multiphase interstellar medium which allows the representation of a co-spatial mixture of cold and hot interstellar medium (ISM) components without introducing scale-dependent parameters. Energy and chemical feedback by Type II and Type Ia SNe, as well as metal-dependent gas cooling (Sutherland & Dopita 1993), are also considered. The model is intended to be as simple as possible and to introduce the fewest input parameters possible. It was specially designed to avoid the inclusion of mass-scale dependent parameters. This makes it suitable for running cosmological simulations where, at any given time, systems of different masses are forming simultaneously. In Scannapieco et al. (2005, 2006) we tested the code by studying the formation of disk galaxies of different mass from idealized initial conditions. Our scheme can reproduce several important effects in galaxy evolution: substantial metal-enhanced galactic winds are produced, redistributing mass and metals and generating a self-regulated cycle for star formation. The galactic winds are generated naturally in our model when the multiphase gas model and SN feedback are both included. This is an important result which allows us to consistently study the formation of galaxies together with the chemical enrichment and the redistribution of matter within the galaxies. Potentially it should also allow investigation of other aspects such as the enrichment of the intergalactic medium. Our model reproduces the expected dependence on galaxy mass: while star formation is suppressed at most by a factor of a few in massive galaxies, in low-mass systems the effects can be much larger, giving star formation an episodic, bursty character. In this paper, we extend the work of Scannapieco et al. (2005, 2006) by studying the formation of disk galaxies in their proper cosmological context. This allows a consistent treatment of processes such as mergers, interactions, inflows, tidal stripping, etc. We thus carry out higher resolution simulations from realistic initial conditions and follow the hierarchical growth of a galaxy similar in size and spin to our Milky Way. We focus on the effects of SN feedback on star formation and on galaxy morphology, emphasizing the dependence of the predictions on input parameters.

Our paper is organized as follows. In Section 2 we describe the simulation code and list the characteristics of our simulations, briefly describing the inputs which are relevant for this work. In Section 3 we explore the effects of SN feedback on star formation (subsection 3.1), galaxy morphology (subsection 3.2) and evolution of specific angular momentum (subsection 3.3). We also study the formation process of the disk components found in our simulated galaxies (subsection 3.4) and the resulting chemical properties (subsection 3.5). In Section 4 we investigate how SN feedback proceeds for smaller galaxies. Finally, we give our conclusions in Section 5.

2 THE SIMULATION CODE

The simulations in this paper were run with the code described in Scannapieco et al. (2005, 2006), which is an extension of the parallel Tree-PM SPH code GADGET-2 (Springel & Hernquist 2002; Springel 2005). The code includes star formation, metal-dependent cooling, chemical enrichment and energy feedback by Type II and Type Ia Supernovae, in addition to a multiphase treatment for the gas component. At the end of this Section, we describe those input parameters of our model that are particularly relevant for the present study, and we refer the interested reader to Scannapieco et al. (2005) for details on the implementation of star formation, chemical enrichment and metal-dependent cooling, and to Scannapieco et al. (2006) for the description of the multiphase gas and energy feedback models. Note that our multiphase treatment and our star formation and feedback models differ substantially from those of Springel & Hernquist (2003) although we do adopt their treatment of the UV background.

We focus on a study of the formation of disk galaxies in their cosmological context. For this purpose we simulate a system with $z = 0$ halo mass $\sim 10^{12} h^{-1} M_{\odot}$, extracted from a large cosmological simulation and resimulated with improved resolution. Our simulation runs from $z = 38$ to $z = 0$ and adopts a Λ CDM Universe with the following cosmological parameters: $\Omega_{\Lambda} = 0.7$, $\Omega_{\text{m}} = 0.3$, $\Omega_{\text{b}} = 0.04$, a normalization of the power spectrum of $\sigma_8 = 0.9$ and $H_0 = 100 h \text{ km s}^{-1} \text{ Mpc}^{-1}$ with $h = 0.7$. The particle mass is 1.6×10^7 for dark matter and $2.4 \times 10^6 h^{-1} M_{\odot}$ for baryonic particles, and we use a maximum gravitational softening of $0.8 h^{-1} \text{ kpc}$ for gas, dark matter and star particles.

At $z = 0$ the halo of our galaxy has spin parameter of $\lambda = 0.03$ and it contains $\sim 1.2 \times 10^5$ dark matter and $\sim 1.5 \times 10^5$ baryonic particles within the virial radius. It was selected to have no major mergers since $z = 1$ in order to give time for a disk to form. Because the selected halo is similar in mass and spin to the Milky Way and has a relatively quiet merger history in the recent past, we thus expect this halo to host a disk galaxy. However, given our incomplete knowledge of galaxy formation processes, this expectation is not necessarily fully correct.

We have run a series of simulations in order to study the dependence of the results on assumed input parameters and to see if the code can produce disk systems. Because of this focus, we decided to vary only the parameters related to star formation and energy feedback, and we fixed those related to chemical enrichment and phase decoupling. In all our simulations we have assumed a SNIa rate of 0.3 relative to SNII and a SNIa lifetime uniformly distributed in the range $[0.1, 1] \text{ Gyr}$. We have adopted the instantaneous recycling approximation for SNII, we have used metal-dependent cooling (Sutherland & Dopita 1993) and we have adopted a Salpeter Initial Mass Function. Chemical yields from Woosley & Weaver (1995) and Thielemann et al. (1993) have been used for SNII and SNIa, respectively. The multiphase gas model of Scannapieco et al. (2006) has been turned on for all experiments. This model *decouples* particles with dissimilar properties, preventing them from being SPH neighbours. In all the simulations presented in this paper, we have used $\alpha = 50$ for the decoupling param-

eter which sets the difference in entropy required for particles to be decoupled (see Scannapieco et al. 2006 for details).

For the star formation and feedback models, there are three relevant input parameters: a) the star formation efficiency c , b) the energy E_{SN} released per SN¹ and c) the so-called *feedback parameter* ϵ_c . In our model, we assume that gas particles are eligible for star formation if they are denser than a critical value ($\rho > \rho_{\text{crit}} = 7 \times 10^{-26} \text{ g cm}^{-3}$ where ρ denotes gas density) and lie in a convergent flow. For these particles, we assume a star formation rate (SFR) per unit volume equal to

$$\dot{\rho}_{\star} = c \frac{\rho}{\tau_{\text{dyn}}}, \quad (1)$$

where c is the star formation efficiency, ρ_{\star} denotes stellar density, and $\tau_{\text{dyn}} = 1/\sqrt{4\pi G \rho}$ is the local dynamical time of the particle. The star formation efficiency then sets the efficiency at which stars are formed or, equivalently, the typical time-scale of the star formation process. Once star particles are formed, they are assumed to give rise to both SNII and SNIa explosions (see Scannapieco et al. 2005 for details on the implementation of star formation and of SN explosions). Each SN event will release an amount of energy, given by the number of exploding stars within the stellar particle multiplied by the energy per SN, E_{SN} . Finally, a feedback parameter is introduced in our model when implementing the transfer of SN energy to the gas. This is based on a separation of gas particles into two phases called *hot* and *cold* (split by assumed thresholds in density and temperature). When SN explosions take place, the energy is distributed as thermal feedback in a fixed proportion to these two phases, the cold phase receives a fraction ϵ_c and the remaining fraction $1 - \epsilon_c$ is distributed to the hot neighbours. While hot particles receive the energy instantaneously, each cold particle instead accumulates the SN energy until it is large enough to raise its entropy to the level of its local hot neighbours. At each time we define for each cold particle a local hot phase and compare the average entropy of the identified hot neighbours with the entropy that the cold particle would have if it absorbed the accumulated energy. This gives the code the flexibility to accommodate itself to local conditions, since different systems will have different typical hot-phase entropies and these will change with time. The parameter ϵ_c is therefore related to the mode of feedback in a non-trivial way (Scannapieco et al. 2006). Together with the values adopted for the star formation efficiency and energy released per SN, the feedback parameter determines the details of the evolution of the galaxy.

A list of the simulations we have carried out is shown in Table 1. They are divided into three series: F, E and C referring to the parameter which is varied in each series. Simulations F were run with different feedback parameter (ϵ_c), simulations E with different energy per SN (E_{SN}) and simulations C with different star formation efficiency (c). Note that F-0.5 is a standard case which belongs to all three groups of simulations. We have also run a simulation without energy feedback (although including chemical enrichment,

¹ In Scannapieco et al. (2006) we used a parameter ϵ_{r} which denotes the fraction of the SN energy assumed to be lost by radiation. In practice, this is equivalent to assume a lower value for E_{SN} . In this work, we decided to use E_{SN} instead of ϵ_{r} .

Table 1. Principal characteristics of our simulations: fraction of energy (and metals) distributed into the cold phase (ϵ_c), energy per SN (E_{SN} in units of 10^{51} ergs) and star formation efficiency (c). We also list dark matter, gas and stellar mass in units of $10^{10} h^{-1} \text{M}_{\odot}$, gas fraction and baryonic fraction both within the virial radius (superscripts '200') and within twice the optical radius (superscripts '2 r_{opt} '). We show the optical radius for the different simulations, in units of $h^{-1} \text{kpc}$. The fraction of stellar mass formed at $z < 1$ is also shown. All quantities are computed at $z = 0$.

Test	ϵ_c	E_{SN}	c	M_{DM}^{200}	M_{gas}^{200}	M_{star}^{200}	f_{g}^{200}	f_{bar}^{200}	r_{opt}	$M_{\text{DM}}^{2r_{\text{opt}}}$	$M_{\text{gas}}^{2r_{\text{opt}}}$	$M_{\text{star}}^{2r_{\text{opt}}}$	$f_{\text{g}}^{2r_{\text{opt}}}$	$f_{\text{bar}}^{2r_{\text{opt}}}$	$f_{*}^{z < 1}$
NF	-	-	0.1	196.4	6.9	24.6	0.22	0.14	12.8	34.8	0.74	14.9	0.05	0.31	0.11
F-0.3	0.3	1	0.1	188.1	5.2	5.6	0.48	0.05	12.5	30.2	0.51	4.4	0.11	0.14	0.16
F-0.5	0.5	1	0.1	190.4	6.2	6.6	0.49	0.06	12.0	29.6	0.37	5.5	0.06	0.17	0.25
F-0.9	0.9	1	0.1	196.2	8.2	7.7	0.52	0.08	15.1	38.9	0.77	6.6	0.10	0.16	0.30
E-0.3	0.5	0.3	0.1	196.4	6.8	16.8	0.29	0.11	11.0	30.3	0.53	12.9	0.04	0.31	0.24
E-0.7	0.5	0.7	0.1	192.9	6.1	9.1	0.40	0.07	10.0	25.6	0.54	7.4	0.07	0.24	0.27
E-3	0.5	3	0.1	187.2	5.6	1.7	0.77	0.04	13.6	31.8	0.27	1.2	0.18	0.05	0.24
C-0.01	0.5	1	0.01	184.1	4.0	11.9	0.25	0.08	8.9	21.5	0.12	9.8	0.01	0.32	0.21
C-0.5	0.5	1	0.5	193.1	7.0	5.6	0.56	0.06	14.5	37.3	0.49	4.4	0.10	0.12	0.31

metal-dependent cooling and the multiphase gas treatment) in order to highlight the effects of this process. This simulation is referred to as NF.

3 IMPACT OF SN FEEDBACK ON THE FORMATION OF GALAXIES

In this Section we use our simulations to investigate how our model of SN feedback affects the formation of a galaxy and, in particular, if this process affects the formation of a disk-like structure. We also analyse the dependence of our results on the values of the relevant input parameters. We will show that SN feedback plays a fundamental role, regulating the star formation rate, pressurizing the gas and allowing its late collapse to a disk structure. In the next Section, we investigate how SN feedback affects the evolution of two galaxies with two and three orders of magnitude smaller mass.

In Table 1 we list a variety of quantities for our simulations: the masses of dark matter, gas and stars (M_{DM} , M_{gas} and M_{star}), the gas fraction f_{g} (i.e. the ratio between the gaseous and baryonic mass), and the baryon fraction f_{bar} (i.e. ratio between baryonic and total mass). All these quantities are computed at $z = 0$ and refer either to the region within r_{200} , the radius enclosing a mean density 200 times the critical value, or to the central regions ($r < 2r_{\text{opt}}$, where r_{opt} is defined as the radius which encloses 83 percent of the baryonic mass of the central object). Note that our haloes are formed by a central system (referred to as the central galaxy) and a series of satellites. Hence, quantities inside the virial radius are affected by the properties of the satellites, whereas those inside twice the optical radius give a cleaner estimation of the characteristics of the central system. In the last column we show $f_{*}^{z < 1}$, which denotes the total stellar mass formed at $z < 1$ divided by the final stellar mass at $z = 0$ (calculated within $r < 2r_{\text{opt}}$).

3.1 Effects on the star formation process

In Fig. 1 we show star formation rates (SFR) for our simulations as a function of time. We have split our plots to

highlight the dependence of the results on each of the input parameters. The top panel shows the SFRs for different ϵ_c values (F-0.3, F-0.5 and F-0.9) and for the run without energy feedback (NF). SN feedback produces a substantial decrease in the SFR, especially at early times. In the no-feedback case, the gas collapses and concentrates at the centre of the potential well, producing a strong starburst which only fades when the amount of available gas decreases. Since there is no mechanism to expel gas in this case, the SFR behaves smoothly following the gas collapse. On the contrary, when SN feedback is considered, the level of SFR is significantly lower at early times and its bursty behaviour indicates the self-regulation of star formation activity produced by the injection of SN energy into the interstellar medium. In this case, each starburst is followed by a depression in the SFR because the expansion of surrounding gas decreases the amount of material available for star formation.

Our results are sensitive to the adopted value for the feedback parameter ϵ_c . For larger ϵ_c values, the cold gas receives more energy, and hence we might expect stronger regulation effects. Note that energy injection to both hot and cold phases affects the evolution of the system. However, the cold gas is the fuel for star formation, and the effects of SN feedback on the SFR are more sensitive to energy deposition in the cold phase. Our results indicate that increasing ϵ_c reduces the SFR at early times but can result in more gas being available for star formation at later phases.

From Table 1 we see that the no-feedback simulation (NF) forms $24.6 \times 10^{10} h^{-1} \text{M}_{\odot}$ of stars inside the virial radius, and $14.9 \times 10^{10} h^{-1} \text{M}_{\odot}$ within $2r_{\text{opt}}$. The difference between these two values reflects the presence of massive satellites which contribute significantly to the stellar mass inside r_{200} ². As a result of efficient cooling and star forma-

² Note that our simulated galaxies are formed by a central system and a series of satellites. In order to have a better estimation of the contribution of satellites to the stellar mass of the simulated galaxy, we have done a proper decomposition of the mass in the halo into a series of subhaloes, and calculated the stellar mass contributed by each of these subhaloes to the total mass. In this way, we find that 25 percent of the total stellar mass is contributed by satellites in the final state of the simulation.

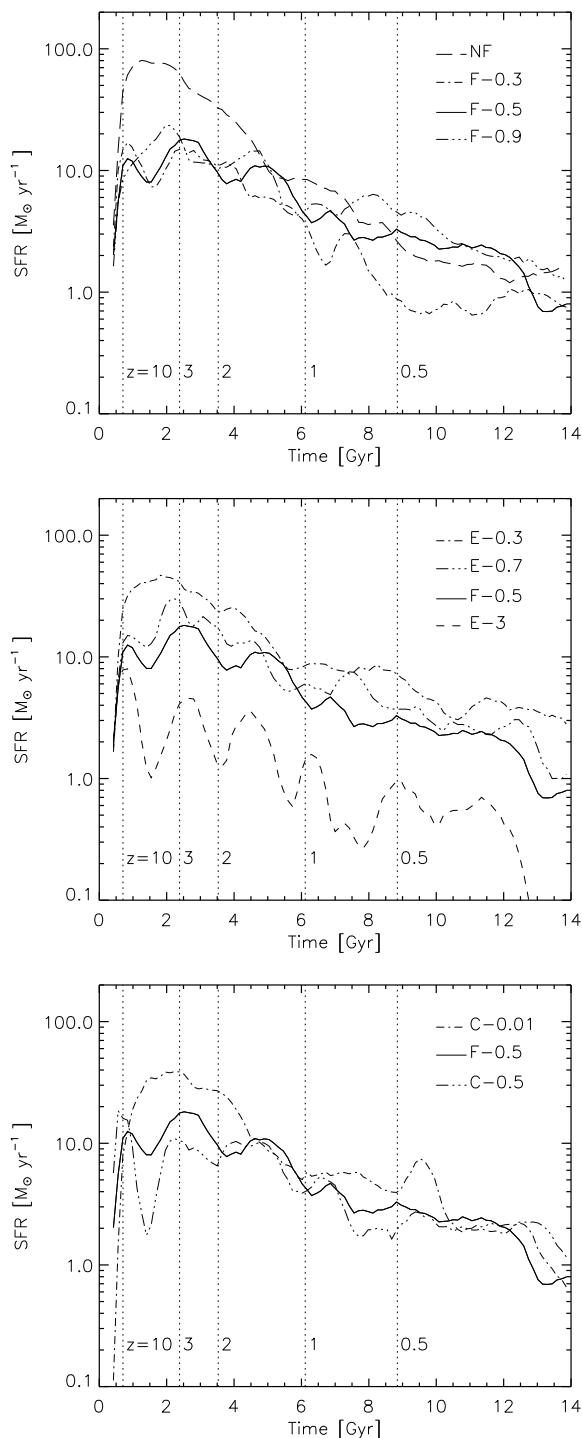


Figure 1. Star formation rates for the three different series of experiments. Upper panel: results for varying feedback parameter (F-0.3, F-0.5 and F-0.9), as well as for the no-feedback simulation (NF). Middle panel: results for varying energy per SN (E-0.3, E-0.7, F-0.5 ($E_{\text{SN}} = 1 \times 10^{51}$ ergs) and E-3). Lower panel: results for varying star formation efficiency (C-0.01, F-0.5 ($c = 0.1$) and C-0.5). Note that F-0.5 is contained in all three series. These star formation rates were calculated using all the stars which ended up within $2 r_{\text{opt}}$ of the centre of the final galaxy. They thus exclude stars which end up in satellite galaxies.

tion, this simulation ends up with only 22 percent of the baryons in the form of gas within the virial radius, and only 5 percent in the inner regions. The inclusion of energy feedback significantly changes these numbers, producing a substantial decrease in the number of stars formed in the galaxy (see Table 1). In our feedback cases, the systems are able to keep ~ 50 percent of the baryons within the virial radius in the form of gas at $z = 0$, and from 5 to 10 percent in the inner regions. Note that in the feedback cases, ~ 80 percent of the stellar mass within the virial radius is in the main galaxy, so the satellites contribute much less to the stellar mass at $z = 0$.

The baryon fraction of the galaxies (listed in Table 1) is also affected by the inclusion of SN energy feedback. In the no-feedback case (NF), $f_{\text{bar}}^{200} = 0.14$ and $f_{\text{bar}}^{2r_{\text{opt}}} = 0.31$, while the feedback cases have $f_{\text{bar}}^{200} = [0.05 - 0.08]$ and $f_{\text{bar}}^{2r_{\text{opt}}} = [0.14 - 0.17]$ which are significantly lower. This is a consequence of galactic winds driven by gas which is heated by the SN energy.

The middle panel of Fig. 1 shows SFRs for the experiments with varying energy per SN. We compare F-0.5 ($E_{\text{SN}} = 1$), E-0.3, E-0.7 and E-3. In this case, higher E_{SN} values translate into lower SFRs and lower final stellar and gas masses (see Table 1). In these cases, the gas fraction within the virial radius increases with the adopted energy per SN, while the baryon fraction decreases. These results are a direct consequence of the higher energy input which prevents further star formation and produces stronger galactic winds. The effects of SN feedback are very clear in the extreme case of very high SN energy (3×10^{51} ergs per SN), where SF occurs in a series of starbursts and its level is very low. We will show in the next subsection that this system is not able to form a realistic disk. In this case, galactic winds are very strong, resulting in a low final stellar mass, and in a baryon fraction which is less than 0.05, both within the virial radius and in the innermost region.

Finally, in the lower panel of Fig. 1 we show SFRs for the series with different star formation efficiencies (c). In the absence of SN feedback, a higher c would simply translate into a higher SFR. However, this is not the case when we consider the injection of SN energy into the ISM. Comparing F-0.5 (with $c = 0.1$) with C-0.01 and C0.5, we find that higher c values lead to lower SFRs and hence lower stellar masses at $z = 0$. This is because for a given gas distribution, larger c values produce more stars and so more SN feedback. The surrounding ISM is thus more strongly heated and reacts by expanding more rapidly. This results in the effective suppression of further cooling and cuts off the gas supply for further star formation. In contrast, a lower c value results in a lower star formation rate and the reduced feedback heating is unable to prevent further cooling of gas into the star-forming phase, with the result that over somewhat longer timescales more stars are formed. It is this competition between SN heating and cooling of gas to provide fuel for star formation which produces the trend between c and the level of SFR in our simulations. For example, run C-0.01 forms twice as many stars as run C-0.5.

We have shown that changing the input parameters of our feedback model produces changes in the SFRs, the stellar masses, and the gas and baryon fractions of the final galaxies. Despite these differences, most of our simulations reproduce approximately the Kennicutt law (Kenni-

cutt 1998) at $z = 0$, with the exception of our no-feedback model and the most extreme and least realistic feedback cases E-3 and C-0.5, which also fail to form disks (see next subsection).

Self regulation of star formation of the kind found in our models is crucial for the evolution of the galaxies. Gas left over from early times as a result of SN energy input can be maintained in a pressure supported halo which later collapses to produce significant star formation activity in the last 8 Gyr ($z < 1$). In the following we will see that this young stellar population is a major contributor to the formation of disks.

3.2 Effects on galaxy morphology

In order to see how SN feedback affects the formation of disks, we now examine the stellar mass distributions of our simulated galaxies. Fig. 2 shows edge-on stellar surface mass density maps at $z = 0$. To make them we compute the total angular momentum of the stars in the central regions ($r < 2 r_{\text{opt}}$), this gives a preferred direction which we define as the z -axis (the angular momentum is positive with this choice). The maps were constructed by projecting the mass distributions within $30 h^{-1}$ kpc in the xy and xz planes. The colors span 4 orders of magnitude in projected density, with brighter colors representing higher densities. The first row shows the final galaxies for different feedback parameters (ϵ_c), the middle row corresponds to different energies per SN (E_{SN}) and the lower row shows galaxies with different star formation efficiencies (c), as well as the no-feedback case. Most of our simulations show significant disks, except for the no-feedback experiment, E-3 (which is not very realistic in terms of the energy produced per SN) and C-0.5.

In order to quantify the properties of our disks we have computed the ratio between the angular momentum of each star in the z -direction (direction of the angular momentum of stars in the central region), j_z , and the angular momentum expected for a circular orbit at the same radius, j_{circ} : $\epsilon = j_z/j_{\text{circ}}$. j_{circ} is defined as $j_{\text{circ}} = r \cdot v_{\text{circ}}(r)^3$, where $v_{\text{circ}}(r)$ is the circular velocity at radius r , $v_{\text{circ}}(r) = \sqrt{G M(r)/r}$, given by the potential well of the system. A disk supported by rotation is characterized by a population of stars with $\epsilon \sim 1$. A component dominated by velocity dispersion will show a distribution peaked near $\epsilon \sim 0$. In Fig. 3 we show histograms of ϵ for our different simulations. The distribution in the no-feedback case (NF) is consistent with a pure spheroidal system. On the contrary, most of our simulations with feedback produce significant disks. Different typical sizes and vertical extensions are found for the disks when the input parameters are varied (see Table 2 where the characteristic sizes are shown). Note that these disks coexist with spheroidal components which, in most cases, dominate the stellar mass of the system. Although the details of the mass distributions depend on the input parameters, it is sig-

nificant that our model produces disks for a wide range of parameters.

We can use our variable ϵ to quantify the properties of the disks and to separate the stars into different components. We have done this considering only particles in the main system and neglecting the satellites to avoid contamination. We decompose the stars in each simulated galaxy into two components which we call *disk* and *spheroid*. We refer to the position of the peak indicative of the disk as ϵ_{peak} . We assume that stars with $\epsilon \geq \epsilon_{\text{peak}}$ are part of the disk, and generate a symmetric distribution around ϵ_{peak} . For a given star with $\epsilon > \epsilon_{\text{peak}}$, we look for a counterpart with $\epsilon' = 2\epsilon_{\text{peak}} - \epsilon$, and with similar height above the disk plane, similar metallicity and similar radius. We repeat this for all stars with $\epsilon > \epsilon_{\text{peak}}$. This procedure avoids ad-hoc parameters and reduces contamination by spheroid stars. As an example, Fig. 4 shows the edge-on and face-on maps of stellar surface mass density for the disk and spheroid components identified in E-0.7. We also show the corresponding velocity fields, clearly contrasting the rotation of the disk with the dispersion-dominated spheroid.

We have applied our method to the runs with extended disk-like components. In Table 2 we show the disk and spheroid masses found for these cases, as well as their ratio. We list the values corresponding to stars within $r < 2r_{\text{opt}}$ of the central galaxy. We also list the half mass radius r_{disk} and half mass height over the disk plane h_{disk} for the disk component. From this table we can see that our experiments have a wide range of disk and spheroid masses. In particular, F-0.5, F-0.9 and E-0.7 show the largest ratios between disk and spheroid mass. In the case of F-0.9, the disk and spheroidal components have the same mass, in all other cases the spheroid dominates in terms of mass (but may not dominate if we consider luminosities⁴). Thus, changing the input parameters leads to a variety of different disk sizes and scale lengths.

In Table 2 we show the time when half of the mass of each component was assembled (τ_{disk} and τ_{spheroid}). In the no-feedback case, the typical scale of star formation is very short, with $\tau_{\text{spheroid}} = 1.17$ Gyr, and the spheroidal components in the feedback cases are also mostly old, with characteristic formation times below 3 Gyr. In the case of the disk components in the feedback experiments, their half mass times indicate that they are young, with typical τ_{disk} of 6 Gyr.

Our star formation and feedback model clearly can produce disks in a cosmological context for any choice of input parameters but spheroid mass dominates over disk mass in all cases in this particular halo, our best case being a 1:1 disk-to-spheroid mass. In the following subsections we choose one of our simulated galaxies and compare its evolution with that of the galaxy formed in the no-feedback case, in order to investigate in more detail how disks form and

³ Note that our definition of ϵ differs from that of Abadi et al. (2004) and Governato et al. (2007), where ϵ is defined as the ratio between the angular momentum of each star in the direction of the total angular momentum of the galaxy and the angular momentum expected for a circular orbit at the same energy.

⁴ By combining the information on the age and metallicity of the stars, we have calculated the disk and bulge ($r < 5 h^{-1}$ kpc) luminosities using the GALAXEV code (Bruzual & Charlot 2003). This yields a disk-to-bulge ratio of 2.4 in the R-band (and a bulge-to-total ratio of 0.30). This is low with respect to observational estimates for Milky-Way type galaxies, particularly in view of the fact that we neglect the effects of dust (e.g. Gadotti 2008).

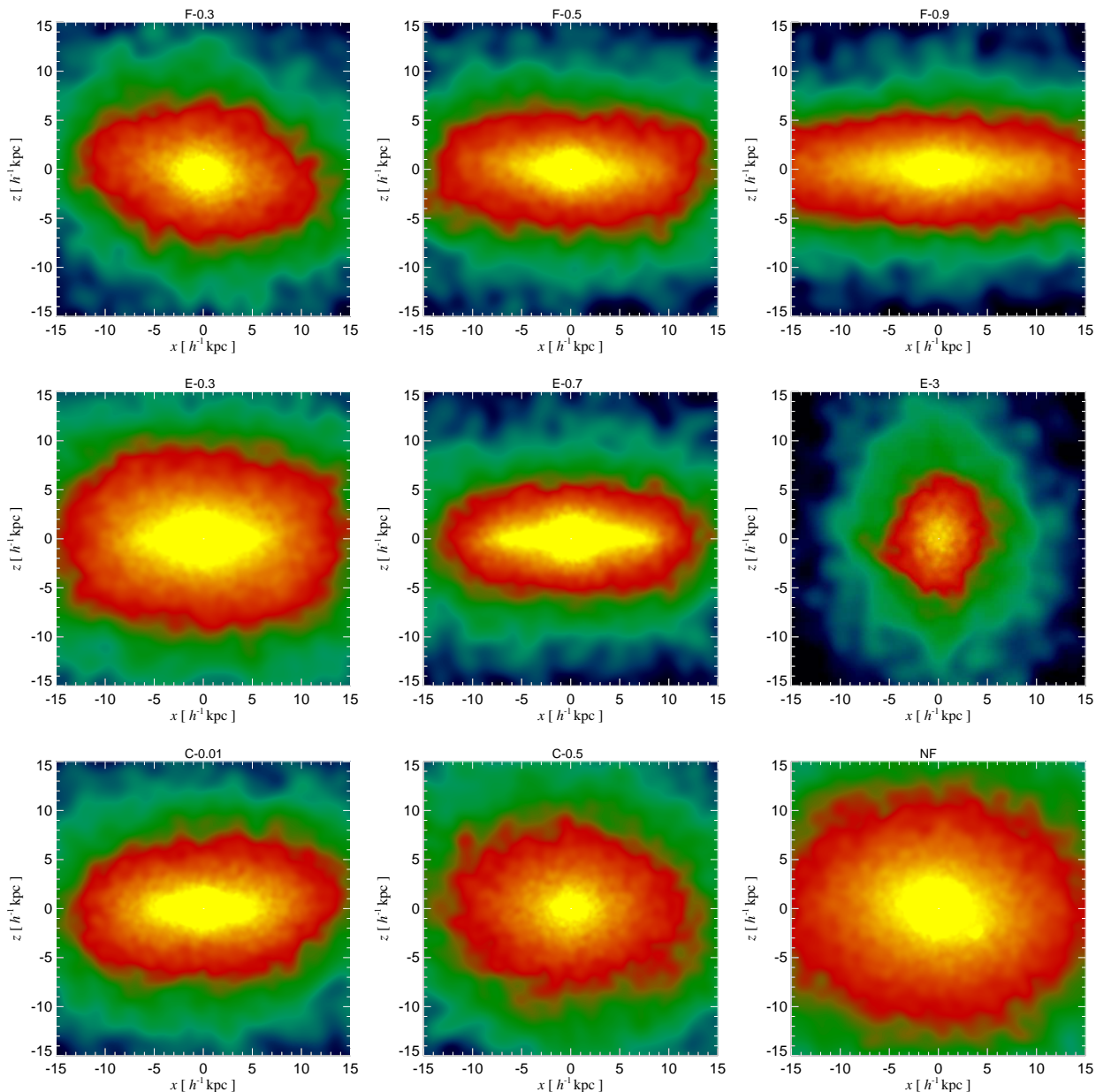


Figure 2. Edge-on stellar surface density maps for 9 different simulations at $z = 0$. The upper panel shows the results for cases with varying feedback parameter (F-0.3, F-0.5 and F-0.9), the middle panel the series with different energy per SN (E-0.3, F-0.5 ($E_{\text{SN}} = 1 \times 10^{51}$ ergs) and E-3), and the lower panel the series with different star formation efficiencies (C-0.01, F-0.5 ($c = 0.1$) and C-0.5), as well as the no-feedback simulation (NF). Note that F-0.5 belongs to all three series.

how SN feedback affects the distributions of specific angular momentum, stellar age and chemical abundance.

3.3 Evolution of the angular momentum

Our model E-0.7 has one of the largest ratios of disk to spheroid mass, and has the thinnest disk. We have selected this simulation as an example to study in more detail the effects of SN feedback in galaxy evolution. The results for this particular simulation are qualitatively similar to those for all other cases where disk-like components formed. In order to investigate why a disk forms with feedback but not

in the no-feedback case (NF) we compare the evolution of the specific angular momentum (i.e. angular momentum per unit mass) in the two simulations. We have computed the specific angular momentum for the dark matter component in the no-feedback and feedback simulations, using particles which ended up within the virial radius at $z = 0$. We followed these particles back in time, calculating their centre of mass and the corresponding specific angular momentum. We have excluded $z = 0$ satellites which contribute an important fraction of the total specific angular momentum at the end, especially in the no-feedback case. We have also calculated the corresponding specific angular momentum for the cold gas plus stars which ended up within $2 r_{\text{opt}}$ at $z = 0$. In this

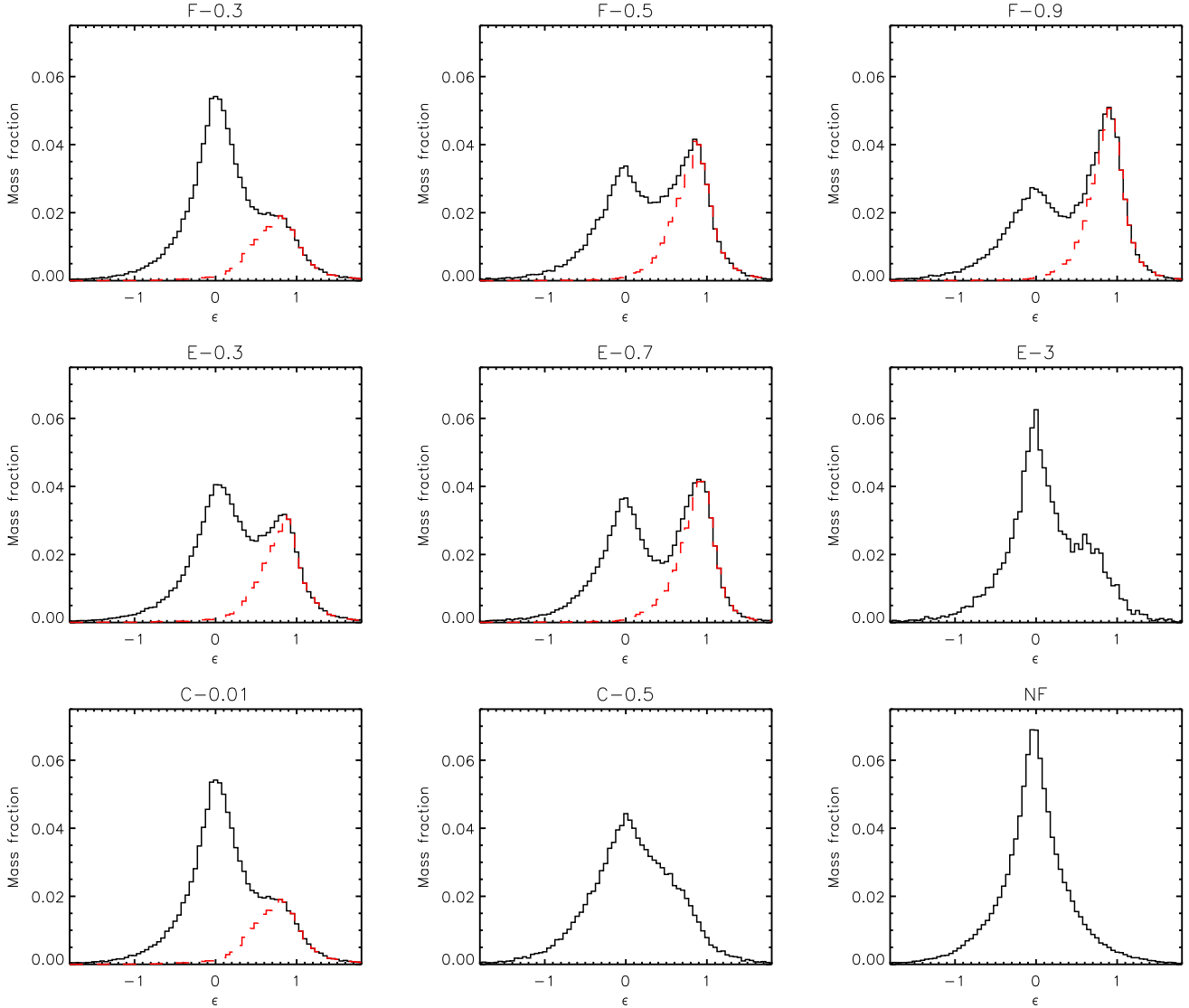


Figure 3. Stellar mass fraction as a function of $\epsilon = j_z/j_{\text{circ}}$ for the different experiments at $z = 0$. The upper panel shows the results for the series with varying feedback parameter (F-0.3, F-0.5 and F-0.9), the middle panel the series with different energy per SN (E-0.3, F-0.5 ($E_{\text{SN}} = 1 \times 10^{51}$ ergs) and E-3), and the lower panel the series with different star formation efficiencies (C-0.01, F-0.5 ($c = 0.1$) and C-0.5), as well as for the no-feedback case (NF). In the cases where a disk-like component is present, we also show the distribution of ϵ for disk stars (dashed lines). In this plot, we only consider stars which belong to the main system (i.e. discounting stars in satellites).

way, we can investigate the relation between the formation of the disk and the evolution of the specific angular momentum of the galaxy.

In Fig. 5 we show results for the evolution of the specific angular momentum of the dark matter and of the cold gas plus stars, calculated as explained above, the left-hand panel shows results for the no-feedback case whereas the right-hand panel corresponds to E-0.7. These plots show that the evolution of the specific angular momentum of the dark matter component is similar in the two cases, growing as a result of tidal torques at early epochs and being conserved from turnaround ($z \approx 1.5$) until $z = 0$.

The specific angular momentum of the cold gas plus stars, however, behaves differently in the no-feedback and feedback experiments, in particular at late times. During the early stages of evolution, the specific angular momen-

tum of this component also grows through the tidal torques exerted by nearby protogalaxies and it maximises at a similar value in the two simulations which is close to the maximum value for the dark matter. However, at later times, the specific angular momentum of the baryonic component behaves differently in the two cases. In the no-feedback case (NF), much angular momentum is lost through dynamical friction, particularly through a satellite which is accreted onto the main halo at $z \sim 1$. The decrease in specific angular momentum after this time is more than an order of magnitude. In E-0.7, on the other hand, the cold gas and stars lose rather little specific angular momentum between $z = 1$ and $z = 0$. Two main factors contribute to this difference. Firstly, in E-0.7 a significant number of young stars form between $z = 1$ and $z = 0$ with high specific angular momentum (these stars form from high specific angular mo-

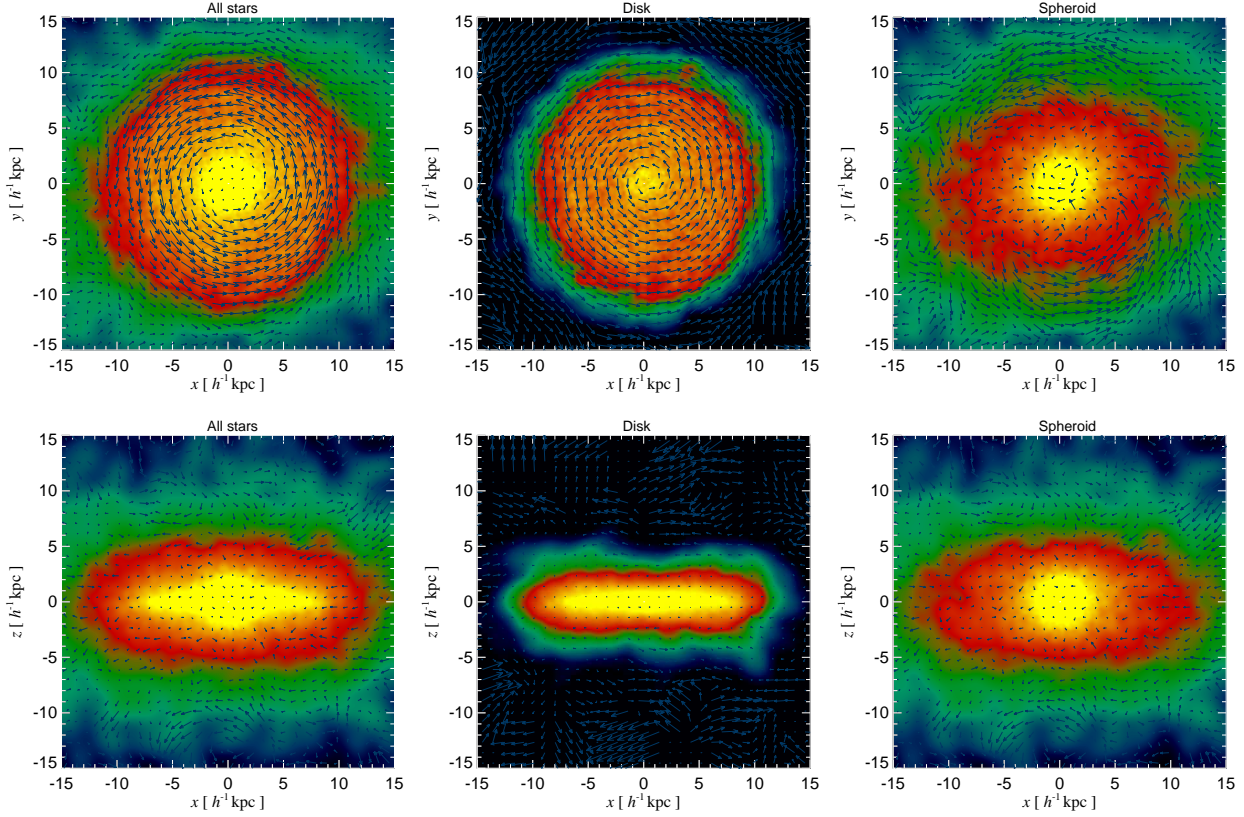


Figure 4. Face-on (upper panels) and edge-on (lower panels) stellar surface density maps for the final galaxy formed in E-0.7. The left-hand panel shows the complete stellar system, while the middle and right-hand panels show views of the disk and spheroidal components, respectively. These maps all have the same color-coding as Fig. 2. The arrows indicate the mean velocity field of the stars. Their lengths scale with velocity.

Table 2. Mass of disk and spheroidal components (in units of $10^{10} h^{-1} M_{\odot}$) and ratio between disk and spheroid masses (D/S) for the different simulations. We also show the disk half mass radius (r_{disk}) and half mass vertical scalelength (h_{disk}) in h^{-1} kpc, as well as the time when half of the final mass of the disk was formed (τ_{disk}) in Gyr, as well as the corresponding time for the spheroid (τ_{spheroid}). We also show the fraction of metals in the stellar ($f_{\text{stars}}^{\text{met}}$) and gas ($f_{\text{gas}}^{\text{met}}$) components and, for the gas component, the fraction of metals within $2 r_{\text{opt}}$ ($f_{\text{gas,in}}^{\text{met}}$) and between $2 r_{\text{opt}}$ and the virial radius ($f_{\text{gas,out}}^{\text{met}}$).

Test	$M_{\text{disk}}^{2r_{\text{opt}}}$	$M_{\text{spheroid}}^{2r_{\text{opt}}}$	D/S	r_{disk}	h_{disk}	τ_{disk}	τ_{spheroid}	$f_{\text{stars}}^{\text{met}}$	$f_{\text{gas}}^{\text{met}}$	$f_{\text{gas,in}}^{\text{met}}$	$f_{\text{gas,out}}^{\text{met}}$
NF	-	14.4	-	-	-	-	1.17	0.99	0.01	-	-
F-0.3	1.29	3.07	0.42	5.82	1.14	4.75	2.95	0.31	0.69	0.26	0.74
F-0.5	2.46	3.00	0.82	6.44	0.84	5.54	2.78	0.22	0.78	0.29	0.80
F-0.9	3.35	3.23	1.04	9.74	0.98	6.24	2.33	0.32	0.68	0.22	0.78
E-0.3	4.85	8.01	0.60	4.75	0.66	5.72	2.54	0.28	0.72	0.28	0.72
E-0.7	3.33	4.05	0.82	5.72	0.50	6.33	2.49	0.20	0.80	0.37	0.63
E-3	-	1.23	-	-	-	-	2.64	0.15	0.85	0.13	0.87
C-0.01	2.71	7.05	0.39	2.64	0.40	4.78	2.83	0.17	0.83	0.21	0.79
C-0.5	-	4.36	-	-	-	-	2.38	0.25	0.75	0.16	0.84

mentum gas which becomes cold at late times); and secondly, dynamical friction affects the system much less than in NF, since satellites are less massive. Our results are similar to those of by Zavala, Okamoto & Frenk (2007), who analysed two simulations with identical initial conditions but differing baryonic physics, one of them resulting in a disk-dominated galaxy, the second in a spheroidal system.

Finally, in the right panel of Fig. 5 we show the final

specific angular momentum of the disk and spheroidal components identified in this simulation at $z = 0$. Clearly the disk component has a high specific angular momentum, comparable to that of the dark matter, while the spheroid formed in this case has a much lower specific angular momentum. This reflects the close relation between angular momentum and morphology.

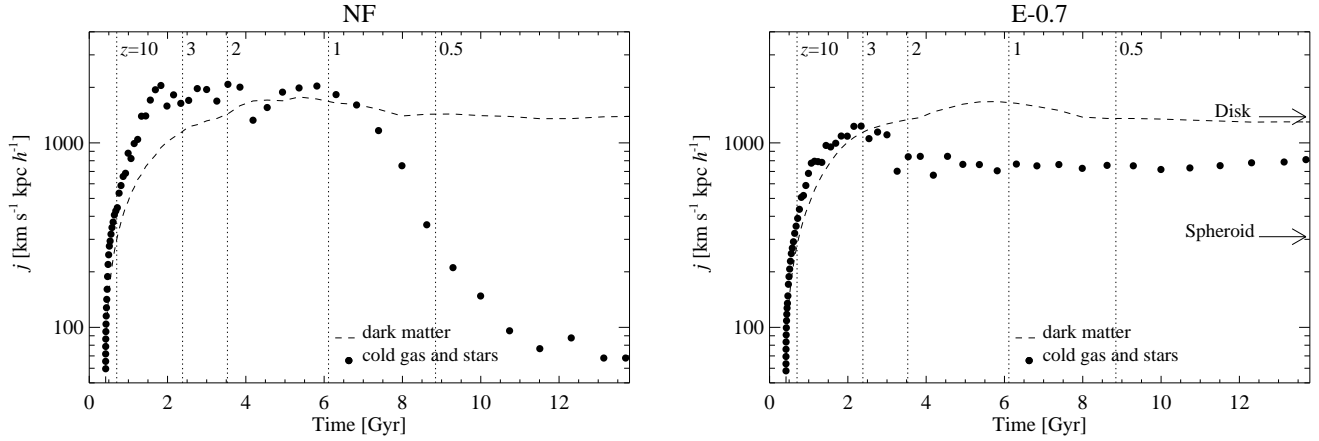


Figure 5. Dashed lines show the specific angular momentum as a function of time for the dark matter that, at $z = 0$, lies within the virial radius of the system for NF (left panel) and E-0.7 (right panel). We also show with dots the specific angular momentum for the baryons which end up as cold gas or stars in the central $20 h^{-1}$ kpc at $z = 0$. The arrows show the specific angular momentum of disk and spheroid stars.

3.4 Stellar age distributions

Our results suggest that the formation of the disks is closely related to the ability to form stars at late times. In our no-feedback experiment, star formation occurs early, giving rise to a stellar spheroid at $z = 0$ which is dominated by old stars. On the contrary, in E-0.7 the stellar component has a larger contribution from young stars. This behaviour is found in all simulations with feedback, as can be seen from Table 1 where we show the fraction of the final stellar mass formed between $z = 1$ and $z = 0$, $f_*^{z < 1}$. The no-feedback simulation has the lowest value for $f_*^{z < 1}$, while the largest values are found for the systems with the most massive disks.

In order to analyse in more detail the relation between disk formation and delayed star formation, we show in Fig. 6 the distribution of stellar formation times for the disk and spheroidal components in E-0.7. The two components differ significantly in their formation times, the spheroid being composed of old stars while the disk contains a younger stellar population. In particular, only 6 percent of the stars in the spheroidal component were formed at times later than 6 Gyr ($z \approx 1$). On the contrary, 53 percent of the final stellar mass of the disk was formed between $z = 1$ and $z = 0$, 24 percent in $z = [0.5, 0]$, and 29 percent in $z = [1, 0.5]$. This suggests that the ability of a system to form a disk correlates with its ability to retain enough gas to form stars at recent times where mergers are not as frequent as at early epochs. This becomes possible when SNe regulate star formation activity. We note that in our simulation without SN energy feedback (NF), only 10 percent of the final stellar mass forms after $z = 1$ (see Table 1).

The age of the disk components can also be quantified by the time when half of the final disk stars had already formed, τ_{disk} . The τ_{disk} values for the different simulations are shown in Table 2. It can be seen that large disks typically have larger τ_{disk} values. In Table 2 we also show the half mass formation time for the spheroidal components, τ_{spheroid} . We find that, in all cases, the spheroids are mainly old. Note that the no-feedback case has the oldest stellar population,

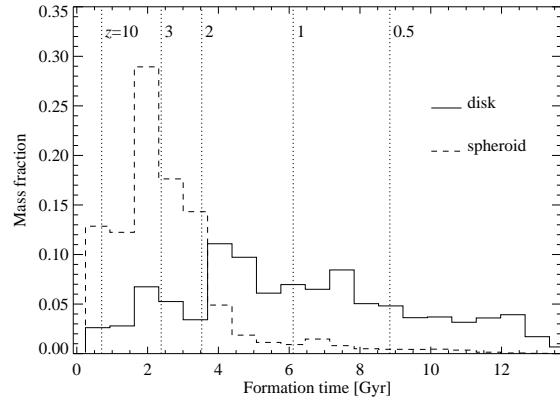


Figure 6. Mass fraction as a function of formation time for stars of the disk and spheroidal components in simulation E-0.7.

while all the feedback cases, independent of the disk they were able to form, show similar values of τ_{spheroid} .

In order to investigate the spatial history of disk assembly, we plot in Fig. 7 the mean formation time of disk stars as a function of radius within the disk plane for E-0.7. We also show the 1σ scatter and we note the times corresponding to $z = 1$ and $z = 0.5$. As noted above, 29 and 24 percent of the final stellar mass of the disk was formed in the redshift ranges $z = [1, 0.5]$ and $z = [0.5, 0]$, respectively. Clearly the stellar disk formed from the inside-out, although the dispersion is high. In fact, we find that star formation between $z = 1$ and $z = 0$ lies primarily in a ring-like structure whose radius increases with time. In contrast, the spheroidal component shows no trend between the age of stars and radius.

3.5 Chemical abundances

In this section we investigate the chemical properties of our simulated galaxies. Metals are produced in stellar interiors and ejected into the interstellar medium when supernova

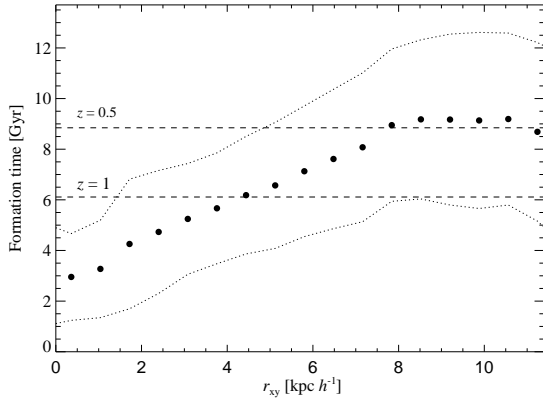


Figure 7. Formation time of disk stars within $2 r_{\text{disk}}$ as a function of distance within the disk plane for the feedback simulation E-0.7. The dotted lines give the $\pm\sigma$ scatter and dashed lines depict the times corresponding to $z = 1$ and $z = 0.5$.

explosions take place. If feedback is neglected, most metals remain locked either in the stars or in the cold gas near star forming sites, since there is no efficient mechanism to transport gas and metals from the inner to the outer regions. Winds generated when SN feedback is included produce a redistribution of mass and metals, and the resulting chemical properties are very different from those obtained when SN feedback is not considered.

Most observations of detailed chemical abundances in stars come from our Galaxy, and are usually quantified separately for the different dynamical components: thin disk, thick disk, bulge and stellar halo. The stellar halo is found to be the most metal-poor component, the thin disk and the bulge are the most metal-rich components (e.g. Ryan & Nories 1991; Chiba & Beers 2000; Zoccali et al. 2003; Nordström et al. 2004). In order to study the chemical properties of our simulated galaxies and to see if we can reproduce these trends, we use the disk-spheroid decomposition explained above. For simplicity, we do not attempt to divide our disk stars into two components. In the case of the spheroidal component, however, we have subdivided the stars into bulge and stellar halo, according to distance from the centre, separating at $5 h^{-1}$ kpc.

In the left-hand panel of Fig. 8 we show the distribution of iron abundance for stars in the bulge and stellar halo for the no-feedback case while the right-hand panel shows similar histograms for E-0.7 together with an abundance histogram for its disk stars. In both simulations the outer part of the spheroid (“the stellar halo”) is shifted to lower metallicities than the inner part (“the bulge”). The shift is more pronounced in the simulation with feedback, although E-0.7 has a lower level of enrichment overall in comparison to the no-feedback case. The disk and bulge components show similar iron abundances in E-0.7, while stars in the stellar halo have lower abundances, in qualitative agreement with observation. Note that the metallicities of the inner stars (i.e. bulge and disk) are the result of chemical evolution in the main galaxy, since these components were mainly formed in-situ. On the contrary, stars in the stellar halo were mostly contributed by satellites and do not reflect the chemical evolution of the main component of the galaxy.

The arrows in the right panel of Fig. 8 indicate how the distributions change for different input parameters. The trends are similar in all cases. An increase in ϵ_c leads to a shift towards higher iron abundance. Note that for higher ϵ_c more metals are dumped into the cold gas from which stars form, leading naturally to higher stellar abundances. On the contrary, increasing the energy per SN decreases the metal abundances because fewer stars are produced and the gas is less enriched where stars do form. As shown before, increasing the SF efficiency leads to lower stellar masses in our model. Consequently, metallicities are also shifted towards lower values in this case.

For the gas component, the resulting metal distribution is affected not only by the metal production itself, but also by the galactic winds which transport an important fraction of the metals outwards, mixing them with the interstellar gas. For strong enough winds, metals can be lost into the intergalactic medium. Hence, many factors influence gas metallicities. In Table 2 we show the fraction of galactic metals which are locked into the stellar and gas components. In the no-feedback case, we find that 99 percent of all metals are locked into stars. This result is because i) most (cold) gas in the central regions has been transformed into stars and hence most metals are locked into the stellar component, and ii) no winds can develop in this case so metals cannot be transported outwards. Consequently, gas in the outer regions (where star formation is less efficient) is not enriched. On the contrary, when our feedback model is included, the fraction of metals locked into stars significantly decreases, being typically of the order of 20 – 30 percent. Because of the efficiency of SN feedback in blowing galactic winds and regulating star formation, most of the metals are now in the gas component.

In order to quantify the importance of winds in distributing metals through the gas component, the last two columns of Table 2 show the fraction of metals in the gas located in the inner regions ($r < 2 r_{\text{opt}}$, $f_{\text{gas,in}}^{\text{met}}$) and in the outskirts of the systems ($2 r_{\text{opt}} < r < r_{200}$, $f_{\text{gas,out}}^{\text{met}}$). In the no-feedback case, only 1 percent of the metals are in the gas. For our feedback cases we find typically that 70 percent of the gaseous metals are outside the innermost region. In Fig. 9 we show the oxygen profiles for the gas components in simulations NF and E-0.7. SN feedback strongly affects the chemical distributions. If no-feedback is included, the gas is enriched only in the very central regions. Including SN feedback triggers a redistribution of mass and metals through galactic winds and fountains, giving the gas component a much higher level of enrichment out to large radii. A linear fit to this metallicity profile gives a slope of $-0.048 \text{ dex kpc}^{-1}$ and a zero-point of 8.77 dex, consistent with the observed values in real disk galaxies (e.g. Zaritsky et al. 1994).

We have shown that our star formation and feedback model produces galaxies with well differentiated stellar dynamical components which also differ in their chemical abundances. In addition, it can produce the correct gas metallicity profiles, although our chemical model is still very simple. Galactic winds produced by SN feedback redistribute metals within galactic haloes. This is an important success of the model. It opens up the possibility of studying the detailed distribution of metals within galaxies forming in their full cosmological context, as well as exploring the enrichment of the intergalactic medium.

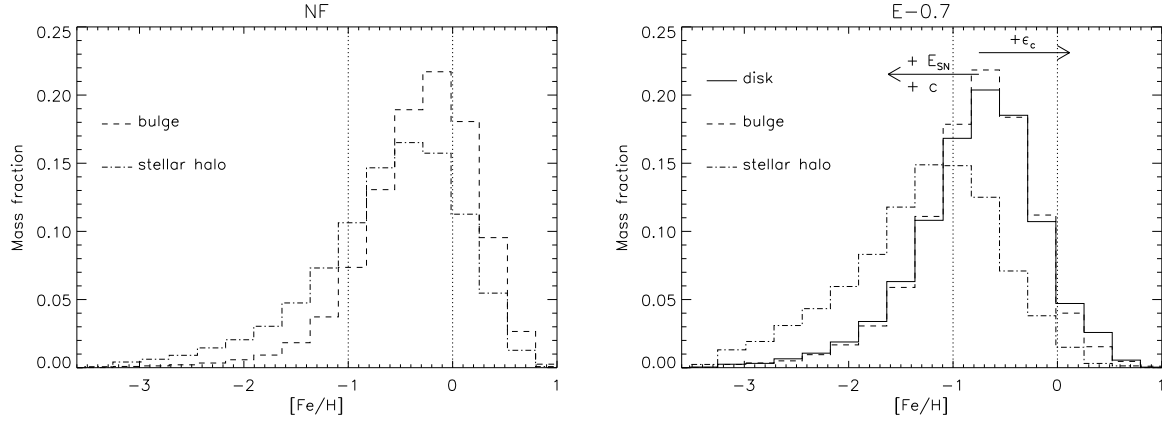


Figure 8. Mass fraction as a function of iron abundance for stars in our no-feedback simulation (NF, left-hand panel), and in E-0.7 (right-hand panel). We show separately the results for stars in the disk (for E-0.7), the bulge and the stellar halo. Vertical lines indicate $[\text{Fe}/\text{H}] = -1$ and $[\text{Fe}/\text{H}] = 0$.

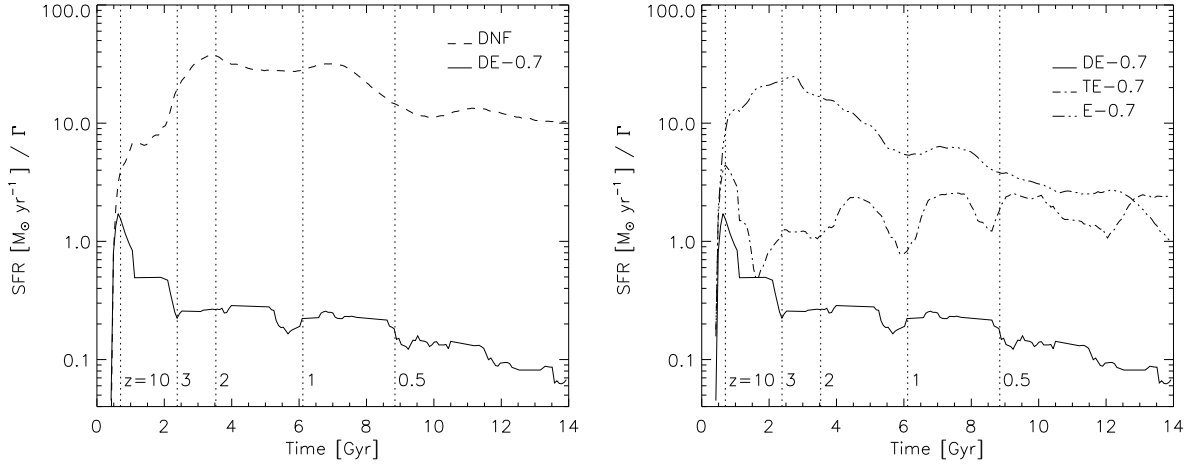


Figure 10. SFRs for simulations of a $\sim 10^9 h^{-1} M_{\odot}$ virial mass system run without (DNF) and with (DE-0.7) energy feedback, as well as for TE-0.7, a $\sim 10^{10} h^{-1} M_{\odot}$ simulation including feedback. To facilitate comparison, the SFRs are normalized to the scale factor Γ .

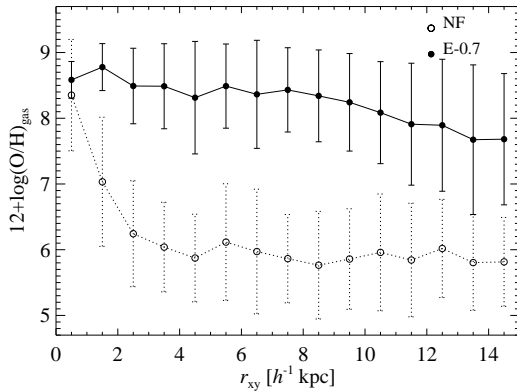


Figure 9. Oxygen abundance for the gas component as a function of radius projected onto the disk plane for our no-feedback simulation (NF) and for the feedback case E-0.7. The error bars correspond to the standard deviation around the mean.

4 DEPENDENCE ON GALAXY MASS

In this Section we investigate how the effects of SN feedback change with galaxy mass. In Scannapieco et al. (2006) we showed that the star formation is affected differently by SN feedback in systems of differing mass. We found that for large systems (virial masses of order $M_{\text{vir}} \sim 10^{12} h^{-1} M_{\odot}$), SN feedback reduces and prolongs star formation with respect to simulations where it is not included. In smaller systems ($M_{\text{vir}} \leq 10^{10} h^{-1} M_{\odot}$), star formation not only decreases but its character also changes, becoming much more bursty. Small systems are very strongly affected by SN feedback, developing galactic winds that are able to expell most of their baryonic mass. In this Section, we again test the effects of SN feedback on smaller mass systems in order to see if the results found in Scannapieco et al. (2006) are valid for galaxies forming in their proper cosmological context.

We have scaled down the initial conditions for simulation E-0.7 by factors of $\Gamma = 10^{-3}$ and 10^{-2} in mass and $\Gamma^{1/3}$ in linear scale to generate two smaller systems of final virial masses $\sim 10^9 h^{-1} M_{\odot}$ (DE-0.7) and $\sim 10^{10} h^{-1} M_{\odot}$.

(TE-0.7). These simulations were run with the same input physics as E-0.7. These initial conditions allow us to compare simulations of galaxies of very different mass but identical assembly history. Note however they may have biased environments and assembly histories compared to real dwarfs. We have also run a simulation of the $\sim 10^9 h^{-1} M_\odot$ virial mass galaxy without energy feedback from SN (DNF). This is a low mass counterpart of NF. In Table 3 we indicate the scale factor Γ , as well as the dark matter, gas and stellar masses of the final $z = 0$ galaxies renormalised by the scale factor for these simulations. This is equivalent to expressing masses in units of $10^7 h^{-1} M_\odot$ for DNF and DE-0.7, and in units of $10^8 h^{-1} M_\odot$ for TE-0.7. We also list the gas and baryon fractions for the final galaxies in these simulations. All these quantities are computed within the virial radius. For comparison, in the lower row we repeat the results for E-0.7 from Table 1. In this way, the results shown in this table can be directly compared; any difference reflects the way SN feedback varies with virial mass.

In the left-hand panel of Fig. 10 we show SFRs renormalized by the scale factor for the $\sim 10^9 h^{-1} M_\odot$ virial mass simulations with and without SN feedback. SN feedback clearly has a dramatic effect on the SFR of such small galaxies. When SN feedback is not included (DNF), the SFR behaves similarly to that in NF (a 10^3 times more massive galaxy), leading to a final stellar mass of $1.88 \times 10^8 h^{-1} M_\odot$. Within the virial radius, the final mass fraction in stars is 0.09 which is comparable to that for NF (0.11). The SFR in DE-0.7 behaves quite differently. It is very low at all times; SN feedback produces a decrease in SFR of about 2 orders of magnitude compared to the no-feedback case. The final stellar mass formed is only $10^6 h^{-1} M_\odot$ (~ 1200 star particles) in this case. The amount of gas within the virial radius is also small, $M_{\text{gas}} = 3.7 \times 10^7 h^{-1} M_\odot$. This is the result of the violent winds that develop in this galaxy due to the shallow potential well. As a consequence, most gas fails to condense and form stars. From the last two columns of Table 3, we can see that the baryons in DE-0.7 represent only 2 percent of the final mass in the galaxy, as opposed to the case without SN feedback where the final baryon fraction is 10 percent.

In the right-hand panel of Fig. 10, we show SFRs renormalised by the scale factor for DE-0.7, TE-0.7 and E-0.7 which differ only in virial mass and were all run with the same SN feedback model with identical input parameters. The effects of SN feedback increase very substantially with decreasing virial mass. Table 3 shows that more massive galaxies at $z = 0$ tend to have larger gas and stellar mass fractions (M/Γ). This is because more of their gas is able to cool and condense to build up the stellar component, and less gas is lost in galactic winds. For these reasons, the larger the galaxy, the lower the final gas fraction (gas over baryonic mass), and the larger the baryon fraction (baryonic over total mass).

We note that poor resolution may affect our results for the smallest galaxy. In Scannapieco et al. (2006) we carried out resolution tests of our feedback implementation. This analysis suggested that small galaxies must be represented by many particles (at least 40000) to get convergent results because their final state is heavily influenced by details of the interplay between heating and cooling. Here our galaxies form through both merging and accretion and it is not

Table 3. List of properties of the simulations with final virial mass $\sim 10^9 h^{-1} M_\odot$ and $\sim 10^{10} h^{-1} M_\odot$. We show the scale factor Γ relative to E-0.7, the dark matter, gas and stellar masses renormalised by the scale factor Γ in units of $10^{10} h^{-1} M_\odot$. We also show the gas and baryonic fractions within the virial radius. For comparison, we show the values for E-0.7 from Table 1.

Test	Γ	$M_{\text{DM}}^{200}/\Gamma$	$M_{\text{gas}}^{200}/\Gamma$	$M_{\text{star}}^{200}/\Gamma$	f_{g}^{200}	f_{bar}^{200}
DNF	10^{-3}	179.5	2.1	18.8	0.10	0.10
DE-0.7	10^{-3}	176.6	3.7	0.1	0.97	0.02
TE-0.7	10^{-2}	185.2	5.2	1.6	0.76	0.04
E-0.7	1	192.9	6.1	9.1	0.40	0.07

clear how much poor resolution at high redshift affects our results at $z = 0$. In the simulations presented in this paper, all the large galaxies, as well as the smaller object DNF, are represented at $z = 0$ by more than 100000 dark matter and 70000 baryonic particles. Only in runs DE-0.7 and TE-0.7 is the number of baryonic particles (17000 and 40000, respectively) so small that better resolution is probably needed to obtain full convergence. However, although the final properties of the systems may slightly differ at higher resolution, our general conclusions about the dependence of SN feedback effects on virial mass should still be valid.

The results obtained in this section prove that our model is able to reproduce the expected dependence of SN feedback on virial mass without changing the relevant physical parameters. Thus, our model is well suited for studying the cosmological growth of structure where large systems are assembled through mergers of smaller structures and systems form simultaneously over a wide range of scales.

5 CONCLUSIONS

We have used a series of simulations of the formation of a galaxy of virial mass $\sim 10^{12} h^{-1} M_\odot$ from cosmological initial conditions to study how SN feedback affects the formation of disks. Our simulations have sufficient resolution to resolve the internal structure of the galaxy as well as large-scale processes such as mergers, interactions, infall, tidal stripping, etc. Our study has focussed on the performance of our SN feedback scheme for realistic initial conditions and on the dependence of the results on the input parameters of the feedback model, as well as on the mass of the galaxy. In the following we summarize our main results.

1) Our model for SN feedback is able to regulate star formation activity by heating and pressurizing gas near star-forming sites. This is reflected in a bursty behaviour for the SFR when feedback is included, particularly in low-mass systems. Different choices for feedback efficiencies produce variations in the star formation levels and in the detailed shape of the SFR, although qualitatively all our simulations show similar behaviour. When compared with a simulation where SN feedback is neglected, the reduction in the final stellar mass formed can be as high as 70 percent even for a Milky Way mass object.

2) Efficient regulation of star formation leads to an increase in the final gas fraction, when compared to a simula-

tion where SN feedback is not included. This, together with substantial mass-loaded galactic winds powered by the SN input, leads to galaxies that, at $z = 0$, have lower baryon fractions.

3) Galaxy morphology is strongly affected by SN feedback. Large disks can be formed and can survive until $z = 0$ if energy injection is allowed. Our results indicate that disks can, however, be formed for a wide range of input parameters. The stellar mass in our galaxies is typically dominated by spheroidal components. In the best case, we found equal masses in the disk and the spheroid. Note, however, that the disk is significantly more luminous since it is significantly younger. We find the final characteristic size and thickness of disks to depend significantly on the input parameters. Adopting too extreme and unrealistic assumptions for the energy per SN or for the efficiency results in failure to form a disk. Similarly, a simulation with no-feedback also leads to a pure spheroidal stellar component.

4) Disks are rotationally supported, have high specific angular momentum and have a substantial number of young stars. Our disks have typical half-mass formation times of ~ 6 Gyr. In contrast, spheroids are old, with half-mass formation times < 3 Gyr. In a simulation without feedback much of the specific angular momentum of the cold component (the cold gas and stars) is lost to dynamical friction during the assembly. As a result, no disk forms.

5) Our disks and spheroids have different chemical properties as a result of their different formation histories. In particular, the stellar halo in our simulations is the most metal-poor component, in agreement with observation, whereas the disk and bulge components have similar near-solar metallicities. Without SN feedback this trend is not recovered and all components show similar, overly high iron abundances. Gas metallicities are also affected by changes in star formation histories and by galactic winds when SN feedback is included. Gas metallicity profiles consistent with observations are only found when feedback is included.

6) In our model, the effects of SN feedback strongly depend on virial mass. We have shown this by scaling down one of our simulations by factors of 10^2 and 10^3 in mass. Feedback has a much stronger effect in smaller systems, where violent galactic winds eject most of the baryonic material and prevent gas from collapsing to make stars. SFRs are low and bursty in such systems. Such small galaxies have lower baryon fractions at $z = 0$ than larger systems.

Our findings show that our model is able to produce realistic disk systems from cosmological initial conditions. This results from the self-regulation of the star formation process and the heating due to feedback which prevents excessive early condensation of gas into the central regions of dark haloes and the consequent later loss of angular momentum. An important success is the fact that disks are obtained for a variety of input parameters, with realistic radial and vertical sizes, and metallicity structures. In all cases we find that the spheroids dominate the stellar mass, suggesting that further refinements are needed if we are to understand the formation of late-type spirals.

ACKNOWLEDGMENTS

We thank the referee, Fabio Governato, for useful comments that helped improve the paper. We thank Adrian Jenkins and Felix Stoehr for making the initial conditions available to us. CS thanks Gabriella De Lucia, Dimitri Gadotti, Klaus Dolag and Sebastián Nuza for useful and stimulating discussions. This work was partially supported by the European Union's ALFA-II programme, through LENAC, the Latin American European Network for Astrophysics and Cosmology. Simulations were run on Ingeld PC-cluster funded by Fundación Antorchas. We acknowledge support from Consejo Nacional de Investigaciones Científicas y Técnicas, Agencia de Promoción de Ciencia y Tecnología and Fundación Antorchas.

REFERENCES

- Abadi M.G., Navarro J.F., Steinmetz M., Eke V.R., 2003, *ApJ*, 591, 499
- Brook C.B., Kawata D., Gibson B.K., Freeman K.C., 2004, *ApJ*, 612, 894
- Bruzual G., Charlot S., 2003, *MNRAS*, 344, 1000
- Cen R., Ostriker J.P., 1992, *ApJ*, 399, L113
- Cen R., Ostriker J.P., 1999, *ApJ*, 519, L109
- Chiba M., Beers T., 2000, *AJ*, 199, 2843
- Dalla Vecchia C., Schaye J., 2008, *MNRAS*, in press (astro-ph/0801.2770)
- Dubois Y., Teyssier R., 2008, *A&A*, 477, 79
- Eke V.R., Efsthathiou G., Wright L., 2000, *MNRAS*, 315, 18L
- Fall S.M., Efsthathiou, G., 1980, *MNRAS*, 193, 189
- Finlator K., Davé R., 2008, *MNRAS*, 385, 2181
- Gadotti D.A., 2008, *MNRAS*, 384, 420
- Gerritsen J.P.E., Icke V., 1997, *A&A*, 325, 972
- Governato F., et al., 2004, *ApJ*, 607, 688
- Governato F., Willman B., Mayer L., Brooks A., Stinson G., Valenzuela O., Wadsley J., Quinn T., 2007, *MNRAS*, 374, 1479
- Hoyle F., 1953, *ApJ*, 118, 513
- Katz N., Gunn J.E., 1991, *ApJ*, 377, 365
- Kay S.T., Pearce F.R., Frenk C.S., Jenkins A., 2002, *MNRAS*, 330, 113
- Marri S., White S.D.M., 2003, *MNRAS*, 345, 561
- Mo H.J., Mao S., White S.D.M., 1998, *MNRAS*, 295, 319
- Navarro J.F., Benz W., 1991, *ApJ*, 380, 320
- Navarro J.F., White S.D.M., 1993, *MNRAS*, 265, 271
- Navarro J.F., White S.D.M., 1994, *MNRAS*, 267, 401
- Nordström B., et al., 2004, *A&A*, 418, 989
- Okamoto T., Eke V.R., Frenk C.S., Jenkins A., 2005, *MNRAS*, 363, 1299
- Okamoto T., Jenkins A., Eke V.R., Quilis V., Frenk C.S., 2003, *MNRAS*, 345, 429
- Oppenheimer B.D., Davé R., 2006, *MNRAS*, 373, 1265
- Peebles, P.J.E., 1969, *ApJ*, 155, 393
- Quinn P.J., Hernquist L., Fullagar D.P., 1993, *ApJ*, 403, 74
- Robertson B., Yoshida N., Springel V., Hernquist L., 2004, *ApJ*, 606, 32
- Ryan S.G., Norris J.E., 1991, *AJ*, 101, 1865
- Scannapieco C., Tissera P.B., White S.D.M., Springel V., 2005, *MNRAS*, 364, 552
- Scannapieco C., Tissera P.B., White S.D.M., Springel V., 2006, *MNRAS*, 371, 1125
- Semelin B., Combes F., 2002, *A&A*, 388, 826
- Sommer-Larsen J., Gelato S., Vedel H., 1999, *ApJ*, 519, 501
- Sommer-Larsen J., Götz M., Portinari L., 2003, *ApJ*, 596, 47
- Springel V., Hernquist L., 2002, *MNRAS*, 333, 649

- Springel V., Hernquist L., 2003, MNRAS, 339, 289
Springel V., 2005, MNRAS, 364, 1105
Stinson G., Seth A., Katz N., Wadsley J., Governato F., Quinn T., 2006, MNRAS, 373, 1074
Sutherland R.S., Dopita M.A., 1993, ApJS, 88, 253
Thacker R.J., Couchman H.M.P., 2001, ApJ, 555, L17
Thielemann F.K., Nomoto K., Hashimoto M., 1993, in Prantzos N., Vangoni-Flam E., Cassé N., eds, Origin and Evolution of the Elements. Cambridge University Press, Cambridge, p.299.
Toth G, Ostriker J.P., 1992, ApJ, 389, 5
Velazquez H., White S.D.M., 1999, MNRAS, 304, 254
Weil M.L., Eke V.R., Efstathiou G., 1998, MNRAS, 300, 773
White S.D.M., 1984, ApJ, 286, 38
Woosley S.E., Weaver T.A., 1995, ApJS, 101, 181
Yepes G., Kates R., Khokhlov A., Klypin A., 1997, MNRAS, 284, 235
Zaritsky D., Kennicutt R.C.Jr., Huchra J.P., 1994, ApJ, 420, 87
Zavala J., Okamoto T., Frenk C.S., 2007, MNRAS, astro-ph/0710.2901
Zoccali M., et al., 2003, A&A, 399, 931